Chapter 3
Materials and Methods - Apparatus Design

Using the literature review as a foundation, this chapter begins with a systematic review of the design criteria necessary to reproduce the motions and loads of actual TKR. System Design, describing the designed and chosen parts of the device, follows in section 3.2. From the loading mechanism to the motion controller, all of the parts and features employed to satisfy each design criteria are described in detail.

3.1 Design Criteria

Based upon the anatomy and motions of the healthy human knee as well as TKR, the desired specifications for the designed apparatus were determined. For simplicity sake and the capability of testing simple geometries instead of actual TKR components, it was desired to load a CoCr disc with a physiologically-correct loading profile on an UHMWPE block to produce line contact representative of condylar contact. Other desired specifications, such as maximum load, sliding distances, and rotation angles, were determined by reviewing the loads and kinematics of the natural healthy knee and TKR, as well as examining the two previously designed simplified testing devices.

3.1.1 Loading Criterion

One primary design criterion was that the designed apparatus be capable of administering a dynamic, cyclical load. Establishing the maximum load of the cycle was crucial in determining the type and size of the loading device required. The maximum knee joint forces of the models developed by Paul (1965) and Morrison (1970) were between 2 and 4 times body weight (BW), with an average of approximately 3.1xBW. For an average150-pound person, 3.1xBW corresponds to 465 pounds (2.1 kN). A cyclic load of 2.2 kN was used in the wear testing conducted by Blunn *et al*. (1991). In conjunction with the information from Paul (1965) and Morrison (1970), it is proposed to incorporate a maximum load of approximately 2.2 kN in our design.

3.1.2 Maximum Contact Stress Criterion

Perhaps more importantly than matching joint forces, reproducing the maximum contact stresses of *in vivo* TKR is essential to producing representative *in vitro* wear. To determine the proper CoCr disc diameter and width, a maximum contact stress must be determined. The maximum contact stresses for various TKR were previously discussed in Section 2.3.2. While data from the literature varied, most of the resulting contact stresses fell between 18 and 23 MPa. Using Hertzian contact equations and by altering CoCr disc size, it is desired to achieve a maximum contact stress within this range.

3.1.3 CoCr Disc Size

The diameter and width of the CoCr disc was modified to generate an acceptable maximum contact stress. An additional constraint placed upon the size of the CoCr disc was the desire to keep the radius of the disc near that of the radii of curvature of common TKR. As previously denoted in Table 2-1, the radii of curvature of common TKR decreases from 48 mm to 20 mm, moving posteriorly. Averaging the two extremes assumes an average radius of 34 mm, or a diameter of 68 mm. Since the maximum joint force during walking occurs at approximately half of the peak flexion angle, the maximum stress using a disc size around the average radius should not differ greatly from the maximum stress seen *in vivo*. Blunn *et al*. (1991) utilized a CoCr disc with a diameter of 71.9 mm, while Wang and coworkers (1999) used a disc having a diameter of 75 mm. By specifying that the disc diameter is in the range of average TKR and appropriate literature, it was anticipated that the kinematics of the designed apparatus would be near that of common TKR.

3.1.4 Motion Criteria

To enable the device to incorporate extreme motion cases, like stair climbing, maximums for the three degrees of freedom (e.g., F/E, AP sliding, and tibial rotation) for the proposed device should be set higher than those reported in Lafortune's testing (1992). Based upon this information, it was decided that allowing up to 120° of flexion, 25 mm of AP sliding, and 30° of tibial rotation would be more than sufficient to accommodate testing of extreme cases. To allow for simple modification of the limits for

individual tests, computer-controlled stepping motors and linear tables were the ideal selection.

3.1.5 Testing Criteria

It is commonly acknowledged that the average person with a total joint replacement walks about 1 million cycles per year (Seedhom *et al*., 1985). To get any significant wear data, TKR materials testing should run for at least this many cycles, if not more. Even with continuous testing at 1 Hz, it would take approximately 12 days to complete 1 million cycles. To obtain fairly quick results and to permit continuous testing, any motors, linear tables, or loading actuators used in our device would need to be capable of a 100% duty cycle.

The most common lubricant used in TKR testing is filtered or diluted bovine (cow) serum (Wang, 1999; Burgess, 1996; Walker, 1997). Wang *et al.* (1999) obtained favorable results using bovine serum with the biaxial line contact wear machine previously discussed in Section 2.6.1. To ensure a low coefficient of friction and lubrication mechanisms similar to those observed *in vivo*, bovine serum was used as the lubricant in the designed testing apparatus.

Multi-station testing allows simultaneous testing of multiple specimens. Consequently, multiple, identical specimens can be tested to ensure similar wear rates and mechanisms. More importantly, if desired, several different materials can be tested simultaneously under the same loading and kinematic conditions. Although multiple stations require greater loading and thus higher load capacity components, it was desired to set up four independent, specimen stations in the device. All of the design criteria previously outlined are summarized in Table 3-1.

Table 3-1. Design criteria for the cyclic sliding wear machine

Design Parameter	Specification
Femoral Component	CoCr disc (OD ≈ 68 – 75 mm)
Tibial Component	UHMWPE block (thickness ≈ 10 mm)
Loading	Physiologically-correct loading
Maximum Load	≈ 2.2 kN
Maximum Contact Stress	18 – 23 MPa
Flexion/Extension	0 – 120°
AP Sliding	0 – 25 mm
Tibial Rotation	0 – 30°
Testing Duration	Up to 1 million continuous cycles
Stations	4
Lubrication	Bovine serum

3.2 System Designs

With the design criteria established, further details of the wear testing apparatus can be developed. With a general concept in mind, selections of a few of the key components were made before any specific part designs. The design and selection of each component and the complete apparatus arrangement are subsequently described.

3.2.1 Loading Mechanism

Although utilizing an external frame was part of the initial concept, any specifics concerning the design of the frame could not be determined until the type of loading application was selected. Whether the load is applied from above or beneath the UHMWPE can make a significant difference in frame construction. As previously mentioned, it was determined that a dynamic, cyclic load of 2.2 kN was to be utilized in the design. Hence, for four stations, a force application of 8.8 kN (1,975 lbf) is required. Taking this high force into consideration, loading from underneath the UHMWPE was preferred to keep the frame supports in tension, and eliminate the chance of frame buckling. The loading configuration is depicted in Figure 3-3.

Applying a dynamic force, especially one as complex as the knee motion profile (refer to Section 2.1.3), required a programmable load source with instant and repeatable response. Consequently, the only viable options to achieve a load of this magnitude were

to use either a hydraulic or pneumatic cylinder with a programmable valve. Due to the high cost of hydraulic components, and because an air supply capable of 105 psi and very high flow rates was already available in the Orthopaedics/Biotribology laboratory (Engineering Science and Mechanics Department, Virginia Tech, Blacksburg, VA), a pneumatic loading system was economically the better option. A standard pneumatic cylinder is shown in Figure 3-1.

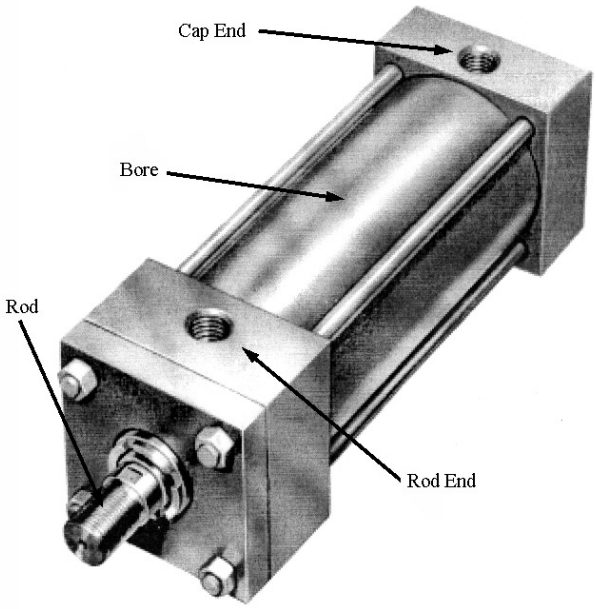

Figure 3-1. Labeled picture of a pneumatic cylinder. The bore label may be misleading; the bore size is actually the interior diameter of the air cylinder (Parker Cylinder Division catalog, Cleveland, OH).

3.2.1.1 Pneumatic Cylinder

The determination of the minimum pneumatic cylinder size was rather simple. By knowing the required maximum force and maximum input pressure, the minimum cylinder diameter was calculated as follows:

$$F = P \cdot A = P \cdot \left(\pi \cdot \frac{D^2}{4} \right) \tag{3-1}$$

and by rearranging Equation 3-1, gives

$$D = \sqrt{\frac{4 \cdot F}{\pi \cdot P}} \tag{3-2}$$

where F = the required maximum force,

P = the maximum input pressure,

A = the area of the cylinder, and

D = minimum cylinder diameter (i.e., bore size).

For the required force of 1,975 pounds (8.8 kN) and an input pressure of 105 psi (0.72 MPa),

$$D = \sqrt{\frac{4 \cdot (1975\,lbs)}{\pi \cdot (105\,psi)}} = 4.92\,inches \tag{3-3}$$

Therefore, a 5 inch bore pneumatic cylinder would be sufficient to supply the required force of 1,975 pounds (8.8 kN).

Since the CoCr discs and the UHMWPE blocks are always in contact during testing, the stroke length of the cylinder was not of great concern. A two-inch stroke was selected to allow ample room to separate the CoCr and UHMWPE, and allow removal of the UHMWPE specimen holder. The rod size was also not of particular concern. A rod of 1-inch diameter was selected, which is more than capable of withstanding the dynamic loading of the system.

Pneumatic cylinders can be either single-acting or double-acting. In single-acting cylinders, a spring pulls the rod back down once the cap end pressure has fallen below a certain minimum. There is less control over output force with single-acting cylinders, yet they are usually more expensive. Double-acting cylinders have air reservoirs on both the rod and cap ends. By keeping the cap end at a fixed pressure and varying the rod end pressure, the desired force output can be obtained. The generated force is simply the rod end pressure subtracted from the cap end pressure, multiplied by the area ($\pi D^2/4$). To minimize cost as well as keep accurate control of the load, a double-acting cylinder was selected.

Since loading occurred from below, the cylinder was bolted to the bottom of the frame, which required a cap end flange mounting configuration. In addition, a cylinder that required no lubrication was preferred to eliminate the chance of contamination of the bovine serum lubricant. Table 3-2 reviews the desired cylinder specifications. The Parker Cylinder Division (Cleveland, OH) was able to meet the desired specifications with the Series 2AN Air Cylinder (part # 5.00HB2ANU19AX2.00).

Table 3-2. Required pneumatic cylinder specifications

5” bore
1” rod
2” stroke
Double-acting
Cap end mounted
Non-lube

3.2.1.2 Par-15™ Series Programmable Valve

To reproduce the rather complex physiologically-correct loading curve, a high-precision, high-flow, programmable regulator was needed. The regulator must be capable of a minimum input of 105 psi and have a minimum flow capacity of 50 SCFM (standard cubic feet per minute). The high flow rate capacity was necessary to quickly fill and exhaust the pneumatic cylinder. In addition, the valve needed to be computer-controlled and have a very quick response to unanticipated changes in pressure.

The only commercially-available valve found to have the required flow capacity and a fairly quick response was the Parker Par-15™ Programmable Valve (Cleveland, OH). A picture of the valve and its specifications are shown in Figure 3-2.

(a)

(b)

Control:	Binary (16 steps)
Flow Capacity:	275 SCFM inlet to outlet 225 SCFM outlet to exhaust
Maximum Inlet:	150 psig
Minimum Output:	6 psig
Output Response:	20 milliseconds
Power Supply:	120/110 V 60 Hz
Solenoid Type:	Normally open
Port Size	½" NPT

Figure 3-2. Photograph (a) and specifications (b) of the Parker Par-15™ Programmable Valve.

The selected Par-15™ valve accepts a binary number between 0 and 15 from the computer, and outputs a desired pressure in increments of 1/15 of the input pressure. Within 20 milliseconds, the pressure begins to change. This digital type of system has its advantages and drawbacks compared to an analog electropneumatic system. Specifically, the Par-15™ eliminates the need for a digital-to-analog converter or an electropneumatic transducer, meaning fewer components, less maintenance, and a direct connection to an I/O card. However, the Par-15™ can only output pressure in steps of 1/15 of the input pressure, whereas an analog system could theoretically output any pressure between zero and the input pressure. Although conceivable that these discrete steps in pressure could make it difficult to precisely reproduce the desired loading curve, with the slight lag in the system due to the compressibility of air, it was anticipated that there would be smooth continuous transitions between steps.

Air from the Par-15™ valve was used to supply the rod end of the pneumatic cylinder, while air of constant pressure, typically equal to the input pressure of the valve, supplied the cap end. The Par-15™ used in the device was specified to be normally-open, meaning that with increasing binary input from zero to 15, the output pressure decreased from the input pressure to the minimum output. Consequently, as previously described, the force output of the cylinder was increased due to the decreasing rod end pressure.

3.2.2 Initial Design Concept

An initial design concept was formulated upon determination of the loading configuration and knowledge that linear tables and motors would be used for precise and flexible motion control. Conceptually, four CoCr discs would be affixed to two steel rods, which would be turned by two geared stepping motors to simulate flexion/extension (F/E) of the knee. A stainless steel tibial tray, sitting atop two motor-controlled tables, would house the UHMWPE samples and the bovine serum lubricant. The two tables would move the tray, simulating AP sliding and tibial rotation. The two tables and the tibial tray would sit atop a steel plate, which would be loaded from below by the pneumatic cylinder, pushing the UHMWPE against the CoCr discs. This initial design concept is more easily understood visually and is depicted in Figure 3-3.

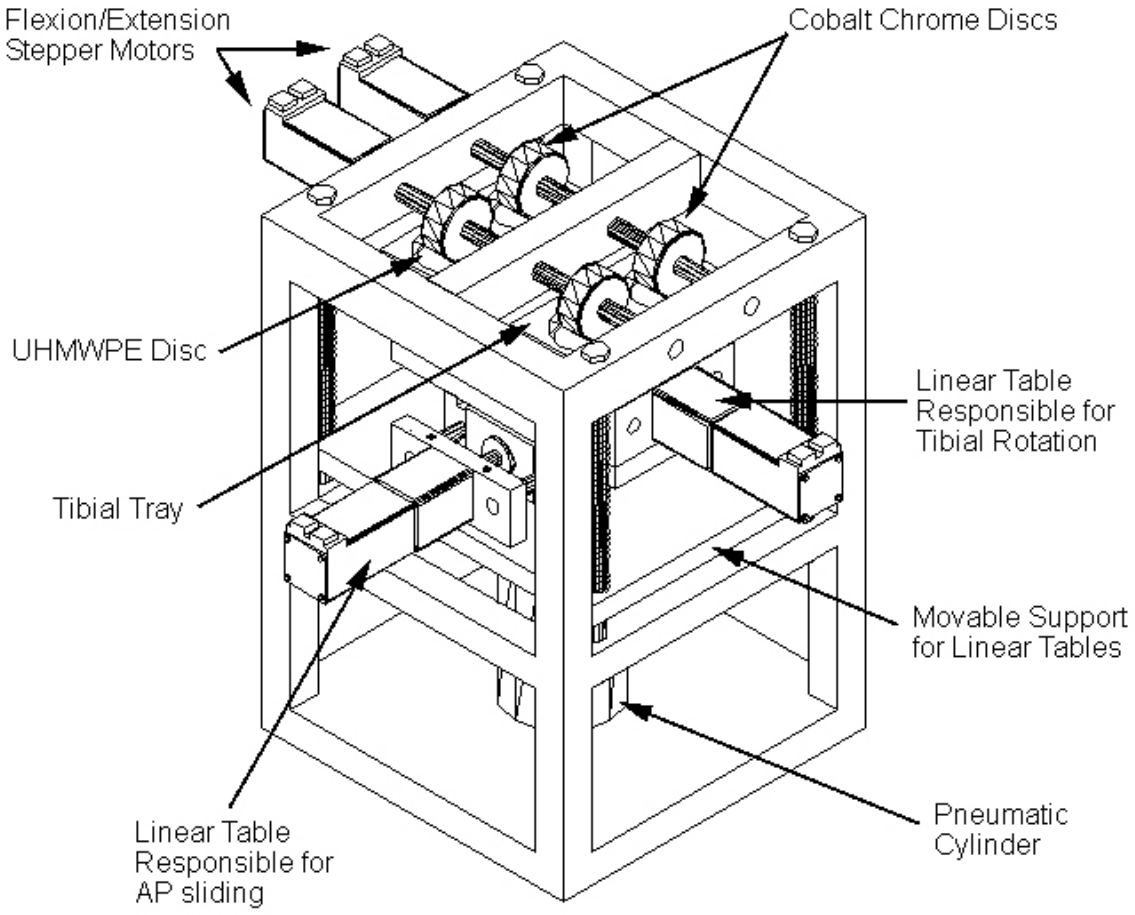

Figure 3-3. Initial design concept drawn in AutoCAD.

Please notice in Figure 3-3 that a linear table is responsible for providing tibial rotation of the UHMWPE tray. While rotation of the tray is not possible with a linear table, this design concept was deliberate and is subsequently explained.

3.2.3 Table Selection

The designed wear testing apparatus required two motion tables to appropriately simulate AP sliding and tibial rotation in the knee. Table selection involved looking at several criteria, such as: load capacity, resolution, repeatability, bearing life, travel rate, and stroke length. With the extremely high dynamic loads desired for the device, load capacity was of foremost importance. The following two sections are devoted to bearing table selection.

3.2.3.1 AP Sliding Table

As previously mentioned (refer to Section 3.1), 25 mm (≈ 1") of AP sliding and a maximum load of 8.8 kN was desired for the apparatus. Before consideration of any other specifications for the linear tables, these two requirements had to be met. A third important criterion was travel rate. Calculating the minimum required travel rate required a review of Lafortune's (1992) AP sliding curve (Figure 3-4).

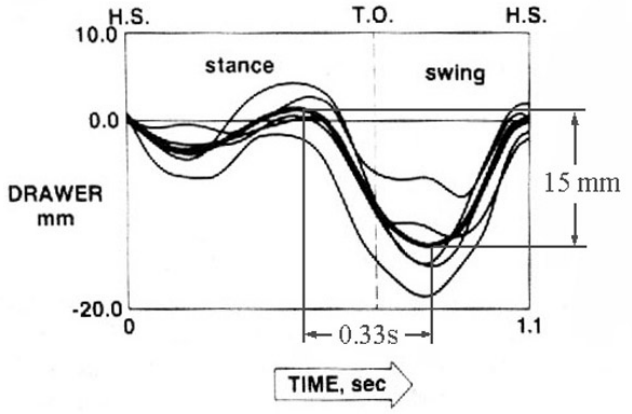

Figure 3-4. AP sliding curve for one walking cycle. The bold line shows the average of Lafortune's five tests (Lafortune *et al.*, 1992).

The quickest movement in the AP sliding curve occurred between the stance and swing phase, in which the tibia slides posteriorly from approximately -1 to 14 mm in about 1/3 of a second. Therefore, the maximum travel rate, V, was calculated as:

$$V = \frac{(-1mm + 14mm)}{1/3\ s} = 45\ mm/s \tag{3-4}$$

Next, if it is assumed during extreme wear testing that the sliding distance may be up to 25 mm in the same amount of time, the minimum required travel rate for the AP sliding table would be 75 mm/s.

Since this table should be designed to run for millions of cycles per test and for a considerable amount of experiments, travel life of the linear tables was also of importance. Travel life for linear tables are measured in the length of total travel. Looking again at Figure 3-4, the AP sliding table would move back and forth approximately 5 mm, and then back and forth 15 mm during each cycle, which equated to 40 mm of travel per cycle. Assuming 1 million cycles per test and 20 tests, the travel life, L, was calculated as:

$$L = (40\ mm/cycle) \cdot (1\ million\ cycles) \cdot (20\ tests) = 1000 km\,. \tag{3-5}$$

Accurate resolution and repeatability of the linear table were not as essential as the previously mentioned four criteria. Since linear tables were used to reproduce motion, rather than align position, distances traveled and travel rate are significantly more important than the actual start and end positions. Repeatability and resolution are discussed in Section 3.2.7. The four primary linear table requirements that were considered in the designed apparatus are summarized in Table 3-3.

Table 3-3. AP sliding linear table requirements

Minimum Load Capacity:	8.8 kN
Minimum Stroke Length:	25 mm
Minimum Travel Rate:	75 mm/s
Required Travel Life:	1000 km

After extensive research and price negotiation, a reasonably priced linear table was found to fulfill the requirements for the apparatus. The Accuslide 2HB from Thomson Industries (Port Washington, NY) (Figure 3-5) met the design specifications. Specifically, model 2HB-M20, at a length of 325 mm, possessed the desired load capacity and travel life. In Figure 3-6(b), the maximum acceptable travel rate for 2HB-M20 is shown in revolutions per minute (rpm). For Thomson Industries' highest resolution ball screw with a diameter of 25 mm and a 5 mm pitch, the maximum travel rate is about 1800 rpm. By multiplying the travel rate by the pitch, and dividing by 60 seconds, the rotational speed of 1800 rpm results in a linear velocity of 150 mm/s, twice that of the desired 75 mm/s minimum. Lastly, the stroke length of the 325 mm model was 85 mm, well over the necessary 25 mm of AP sliding (Thomson Industries catalog).

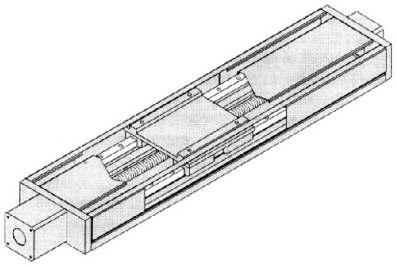

Figure 3-5. Drawing of the Accuslide 2HB linear table from Thomson Industries.

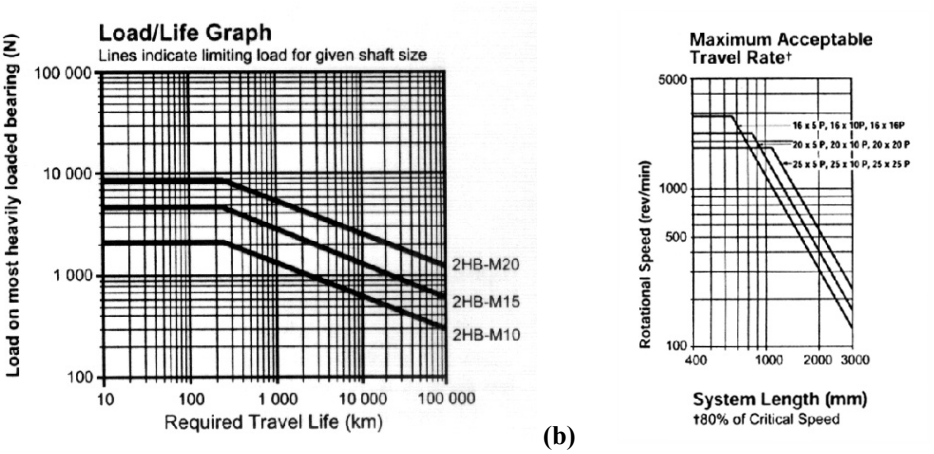

Figure 3-6. Load/life (a) and travel rate (b) graphs for the Accuslide 2HB. The load/life graph (a) shows that at 9 kN, the 2HB-M20 has a travel life of 300 km. However, the average load applied will actually be less than half of that, giving the 2HB-M20 a travel life of around 2000 km. (Thomson Industries catalog, Port Washington, NY)

After selection of the AP sliding table, specifications and complications of selecting the table responsible for tibial rotation were addressed.

3.2.3.2 Tibial Rotation Table

The table responsible for tibial rotation, shown in the initial design (Figure 3-3), was actually a linear table. This was not some ingenious design scheme. In reality, a commercially-available rotary table with the required load capacity (1,975 pounds) could not be found. For instance, the highest load rotary table available from Parker-Daedal (Harrison City, PA) had a direct loading maximum of only 200 pounds.

While the lack of rotation was a considerable setback, it did not mean that tibial rotation could not be simulated in the design. As mentioned briefly in Section 2.6.2, tibial rotation is necessary to induce cross-shearing of the UHMWPE, and thus, prevent orientation of the UHMWPE molecular chains. With TKR, the stresses responsible for cross-shearing cross at an angle of about 10° (Wang *et al*., 1999). Thus, as long as the UHMWPE did not follow the same path moving forward as it did on its return, it was possible to achieve cross-shearing at this angle utilizing a linear table. Based upon this development, it was decided to move the tray in a narrow figure-eight or bow-tie configuration to generate the necessary cross-stresses.

3.2.4 CoCr Disc Size

The size of the CoCr disc has a significant effect on the resulting kinematics, contact area, contact stress, and thus, wear of the UHMWPE. As stated earlier, it was desired to keep the radius of the CoCr disc close to the radii of curvature of common TKR, and close to that of the CoCr discs used in the simplified devices previously discussed (68-75 mm). By maintaining similar curvature, it was anticipated that the kinematics of the testing apparatus would be near those of *in vivo* TKR.

Reproducing the maximum contact stresses seen *in vivo* may be more essential to initiating proper wear mechanisms than matching TKR kinematics. The maximum contact stress in the testing was estimated by applying Hertzian contact equations for a cylindrical CoCr disc on a flat UHMWPE block.

There are several main assumptions in Hertzian contact theory: (i) the contacting surfaces are assumed frictionless, (ii) strains are considered small, (iii) contacting surfaces are assumed continuous, and (iv) both surfaces deform (Lewis, 1998). With the low coefficient of friction of TKR, the first assumption was regarded as fulfilled. The second assumption was fulfilled, considering that the displacements encountered in TKR are very small due to the high moduli of elasticity of the two materials. The contacting surfaces are certainly planar, so the third assumption above holds true. The last assumption that both of the contacting surfaces deform, however, may not be satisfied in this case (Lewis, 1998). In TKR, only the UHMWPE is considered to deform, which may be a drawback to this method. However, elasticity methods, like Hertzian contact theory, have been shown to predict contact stresses of TKR close to those predicted using finite element analysis and Fuji pressure sensitive film (Bartel *et al*., 1986); therefore, Hertzian equations were used to predict the contact stresses for the CoCr/UHMWPE interface.

Hertzian equations for a line contact were used to find the contact width and the mean and maximum contact stresses between two loaded bodies of radii, R_1 and R_2, moduli, E_1 and E_2, and Poisson's ratios, ν_1 and ν_2. Equations 3-6 and 3-7 were used to find the effective curvature, R, and contact modulus, E*, of the two bodies:

$$\frac{1}{R} = \frac{1}{R_1} + \frac{1}{R_2} \quad \text{and} \tag{3-6}$$

$$\frac{1}{E^*} = \frac{1-\nu_1^{\,2}}{E_1} + \frac{1-\nu_2^{\,2}}{E_2} \ . \tag{3-7}$$

Equations 3-8, 3-9, and 3-10 were used to calculate the semi-contact width, a, the mean contact stress, σ_{avg}, and the maximum contact stress, σ_{max}, respectively:

$$a = 2 \cdot \sqrt{\left(\frac{P \cdot R}{w \cdot \pi \cdot E^*} \right)} \tag{3-8}$$

$$\sigma_{avg} = \frac{P}{2 \cdot w \cdot a} \tag{3-9}$$

$$\sigma_{\max} = \frac{4 \cdot \sigma_{avg}}{\pi} \tag{3-10}$$

where P was the applied load and w was the width of the CoCr disc.

Applying the Hertzian contact equations with known material properties of CoCr and UHWMPE and the known maximum load of 2.2 kN, we were able to estimate maximum contact stresses for varying diameters and widths of the CoCr disc (Table 3-4).

Table 3-4. Resulting contact stresses for varying CoCr disc radii and widths using Hertzian contact equations.

CoCr diameter, 2·R (mm)	CoCr width, w (mm)	Average Contact Area (cm^2)	Maximum Contact Stress (MPa)
63.5	25	1.46	19.1
68.0	25	1.51	18.5
72.0	25	1.56	18.0
75.0	25	1.59	17.6
76.2	20	1.43	19.5

Constants: P = 2.2 kN, E_{CoCr} = 200 GPa, ν_{CoCr} = 0.3, E_{UHMWPE} = 0.5 GPa, ν_{UHMWPE} = 0.4, and $R_{UHMWPE} = \infty$ (flat). References for material properties of CoCr & UHMWPE.

Although it was originally desired to maintain similarity in the radii of curvature for the CoCr discs as previously used (Wang et al., 1999; Blunn et al., 1991), finding CoCr bar stock of these radii proved difficult. In fact, the largest outer diameter bar of medical grade CoCr (ASTM F799) that could be found was a 2 1/2" (63.5 mm) diameter bar from Carpenter Specialty Alloys (BioDur® Carpenter CCM Plus, Reading, PA). Using this diameter with a disc width of 25 mm and applying the Hertzian contact equations yielded a maximum contact stress similar to those seen in the literature (Table 3-4). It was believed that this radius was close enough to those of implanted TKR, so that the accurate replication of *in vivo* kinematics was not compromised.

3.2.5 UHMWPE Tray

As previously mentioned, it was desired to accommodate multiple samples within the specimen holder for multi-station testing. Based upon arbitrary size restrictions, it was decided that the tray supporting the UHMWPE should house four specimens.

Additionally, during testing, these chambers hold lubricant, specifically bovine serum. Consequently, to avoid the possibility of corrosion and ionic contamination of the serum, the UHMWPE tray was manufactured from stainless steel (SS). Stainless steel is highly corrosion resistant, and based upon its material properties is capable of enduring the high loads and stresses encountered during testing (The Hendrix Group, Houston, TX).

Based upon a review of the literature and commercially-available TKR, the UHMWPE specimens should have a thickness between 10 and 12 mm. The surface dimensions of the UHMWPE also play a significant role in the amount of UHMWPE wear. Specifically, if the width of the UHMWPE specimen is larger than the width of CoCr disc, the edges of the CoCr disc can cut into the UHMWPE, which increases wear rates and creates wear mechanisms not seen among *in vivo* TKR. One way to minimize edge effects is to use a narrow, rectangular specimen of UHMWPE, however, the decreased UHMWPE width can significantly increase the contact stress. In addition, machining of a rectangular specimen and a rectangular notch to hold the specimen was significantly more expensive than simply machining a circular hole to house a cylindrical piece of UHMWPE. To reduce machining costs and minimize edge effects, cylindrical UHMWPE discs were used in addition to rounding the edges of the CoCr discs used in the device.

Another necessary feature was that the UHMWPE tray must accommodate simple removal of the UHMWPE specimens for post-testing procedures. Consequently, the tray was designed to attach to the upper linear table by six small screws, allowing easy removal of the entire tray from the apparatus. Additionally, notches were machined next to and underneath the UHMWPE specimens, so the UHMWPE could be easily pried out of the tray with a screwdriver or similar tool. An Autodesk Inventor™ (San Rafael, CA) rendering of the UHMWPE tray is shown in Figure 3-7.

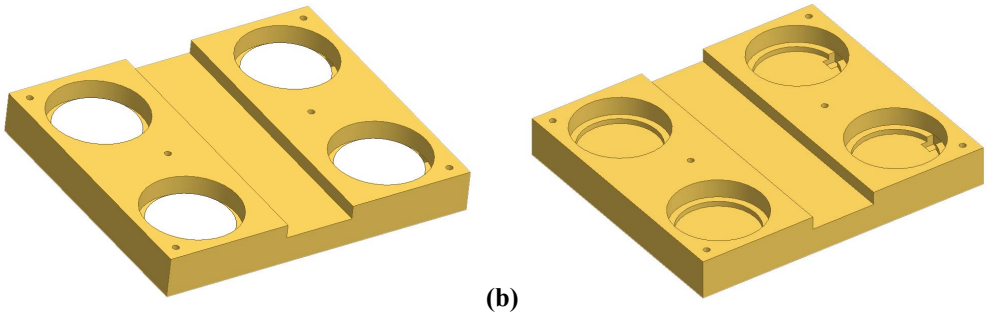

(a) (b)

Figure 3-7. Autodesk Inventor™ representation of the SS UHMWPE tray with (a) and without (b) the UHMWPE specimens.

The depth and size of the specimen bores was dependent on the UHMWPE thickness, the radius of the CoCr disc, and the length of AP sliding. Also, it is crucial that the depth was great enough to avoid splashing of the bovine serum from the specimen chamber during testing. Knowing the CoCr disc diameter (63.5 mm/2.5"), UHMWPE thickness (10 mm/0.39") and AP sliding distance (25 mm/0.98"), intuition and simple trigonometry was used to determine favorable dimensions of the specimen chambers. An inner bore with a depth and diameter of 0.9" (22.9 mm) and 3.0" (76.2 mm), respectively, and an outer bore diameter of 3.5" (88.9 mm) were found to be suitable for the application. To accommodate four specimen chambers, the tray was determined to be 11.5 x 10.0 x 1.5 inches. A tray with these dimensions allowed enough room for AP sliding and enough depth to avoid splashing of the serum. The size of the tray and the locations of the chambers were calculated to allow equal loading of the CoCr discs on each UHMWPE specimen.

3.2.6 Apparatus Frame Design

The initial frame structure, shown in Figure 3-3, was designed to accommodate the motions of the pneumatic cylinder and the linear tables, and equally distribute the load to all four discs. Proper dimensions of the frame and its structural components were necessary to allow accommodation of the UHMWPE tray, adequate movement of the tray and the pneumatic cylinder, and an appropriate factor of safety against static and dynamic frame failure.

3.2.6.1 Frame Height

First, the frame height must be calculated to ensure proper fit of all the components and allow for enough space to easily remove the UHMWPE tray. One correction to the original frame design was to change the sleeve bearings for the F/E rods to pillow block bearings for easier insertion and adjustments of the rods. These bearings were hung from the top of the frame, which needs to be taken into consideration to determine the appropriate frame height. The minimum height of the frame was determined by simply adding the heights of all of the components and supports between the bottom plate and the top bars. The maximum frame height was the summation of the minimum frame height and the cylinder stroke length. Given in Table 3-5 are the dimensions used to determine the desired frame height.

Table 3-5. Dimensions used in the calculation of the minimum and maximum frame heights

Component	Height (inches)
Bottom Plate	1.500
Pneumatic cylinder	+ 8.500
Table support	+ 1.500
AP sliding table	+ 3.465
Tibial rotation table	+ 3.465
Tray support	+ 1.000
Tray spacer	+ 0.500
UHMWPE tray	+ 1.500
Pillow block bearing (1/2 height)	+ 1.063
CoCr disc radius	+ 1.250
Top bars	+ 2.250
Sink distance from top of tray to UHMWPE	- 0.506
Minimum height	**25.487**
Cylinder stroke length	+ 2.000
Maximum height	**27.487**

Ideally, the chosen frame height should be nearly the maximum allowable, leaving plenty of room for the removal of the UHMWPE tray, while still initiating contact between the CoCr and the UHMWPE. Over time, however, wear and compressibility of the UHMWPE may leave gaps between the two materials. Also,

continually pushing the cylinder against the rod end at maximum stroke length could be result in damage to the pneumatic cylinder. Consequently, a frame height of 27 inches, slightly below the maximum allowable, was chosen to avoid these potential problems.

3.2.6.2 Frame Width and Depth

The width and depth of the frame are only dependent on the UHMWPE tray and its distances of motion. As stated earlier, the UHMWPE tray is 11.5 x 10.0 x 1.5 inches. To allow for AP sliding and the simulated tibial rotation, the tray and the tables must be able to move 25 mm (1") in either direction in the horizontal plane. An interior space of 13 x 13 inches was allocated to allow plenty of room for movement.

3.2.6.3 Structural Components

The bars and plate components of the apparatus frame were constructed from cold-rolled steel (BMG Metals, Richmond, VA) for its high strength and relatively low material costs. Initially, all of the bars were designed to be 1.5 x 1.5 inches square, with the bottom plate being 1.5 inches thick. These initial estimates were a starting point to evaluate structural integrity. Static and evaluation (refer to Section 3.2.6.4) showed that the frame with these components was structurally stable. Although the bar thickness could have been significantly reduced without compromising an appropriate factor of safety, since the material costs are almost negligible (1/10 the cost) compared to the machining costs, the bars were left at 1.5 x 1.5 inches to ensure superior stability and minimal frame displacement. In addition, the larger bars would yield a heavier frame, presumably, reducing frame vibration during testing. The only change in bar size from the original estimate of 1.5 x 1.5 inches was with the top bars. These bars were made to be 1.5 x 2.25 inches to reduce displacement at the top of the frame, where the bearings for the F/E rods would be attached. All of the frame's components' sizes were now determined (Figure 3-8) and the frame was statically analyzed.

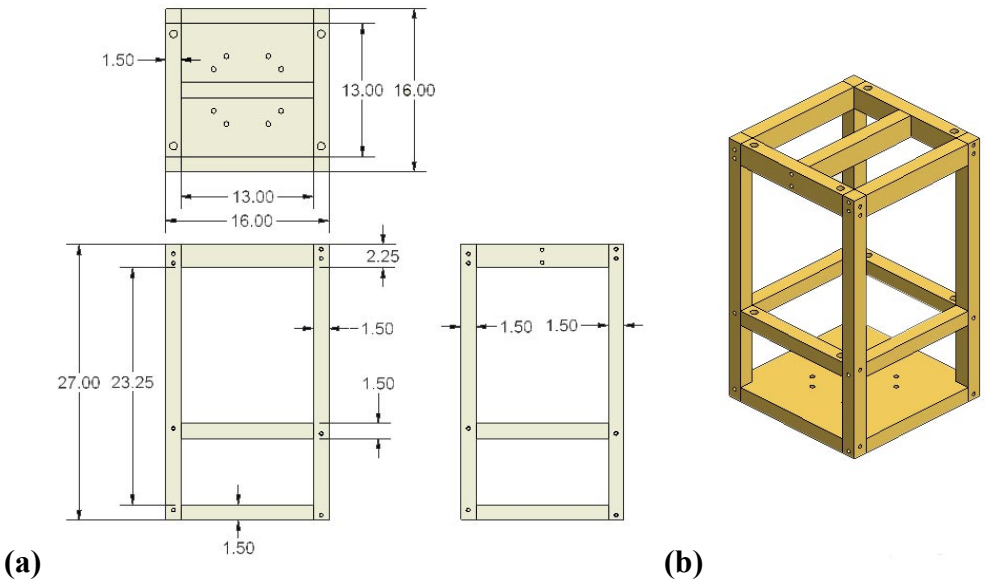

Figure 3-8. Structural components and basic dimensions of the apparatus frame. The two-dimensional drawing (a) showing (clockwise from the top) the top, right, and front views, and an isometric rending (b) of the assembled frame were drawn in Autodesk Inventor™.

3.2.6.4 Finite Element Analysis of the Frame

With the dimensions of the frame determined, the frame was imported into IDEAS CAD software (SDRC, Milford, OH) for finite element analysis (FEA). Although the assembled frame would actually consist of bolted bars, for simplicity, the frame for the FEA was imported as one solid piece of steel. Even though this assumption would eliminate stress concentrations at the bolt sites, it was anticipated that a tightly bolted frame would respond similarly to a solid frame. For this study, FEA was used only to estimate the stresses and displacements in the frame. Additionally, if the FEA resulted in a large enough factor of safety, it could be concluded that the frame would be structurally stable even with bolted components.

The first step in the FEA was to produce the mesh for the frame. Given a specific element size, IDEAS software automatically creates the frame's mesh. After several attempts, an element size of one inch was specified to give accurate results without overloading computer memory and significantly increasing solution time. The resultant mesh produced by IDEAS is shown in Figure 3-9.

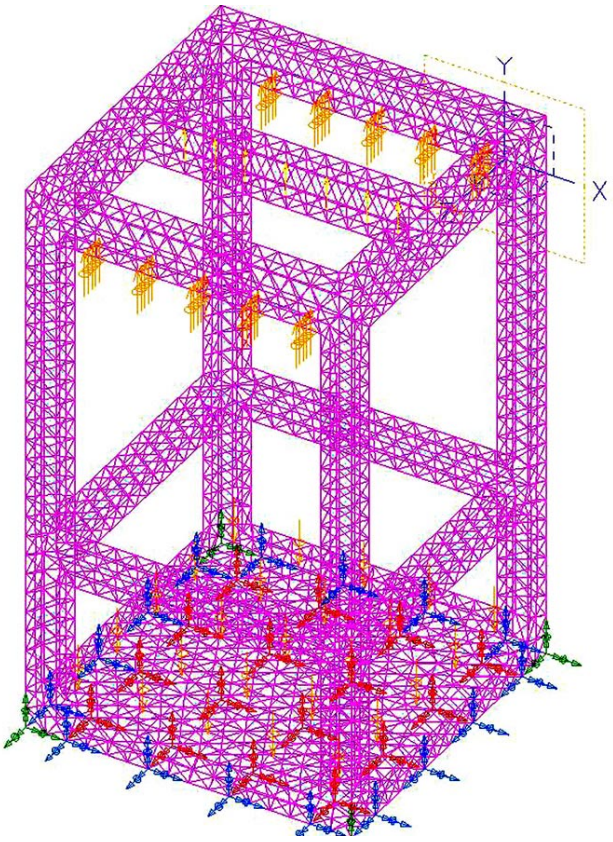

Figure 3-9. FEA mesh of the imported frame with 1" elements and boundary conditions (IDEAS).

The mesh shown in Figure 3-9 is for the simple case of vertical loading at 2000 pounds. Appropriate boundary conditions were inserted to ground the bottom plate. With the mesh completed, solutions for stress and displacement in the frame were found. The visual output of the FEA solution is shown in Figure 3-10. As noted, the IDEAS solution visually depicted the various stresses in the frame and determined the maximum stress and displacement in the frame. When the frame was vertically loaded with 2000 pounds, the maximum stress was determined to be 1.64 ksi. Since cold-rolled steel has a yield strength of 70 ksi (BMG Metals), there is factor of safety over 40 against yielding of the steel during pure vertical loading. To give the reader a better appreciation of the locations where buckling would occur based upon the FEA, an exaggerated version of the displacements of the frame when vertically loaded with 2000 pounds is shown in Figure 3-11.

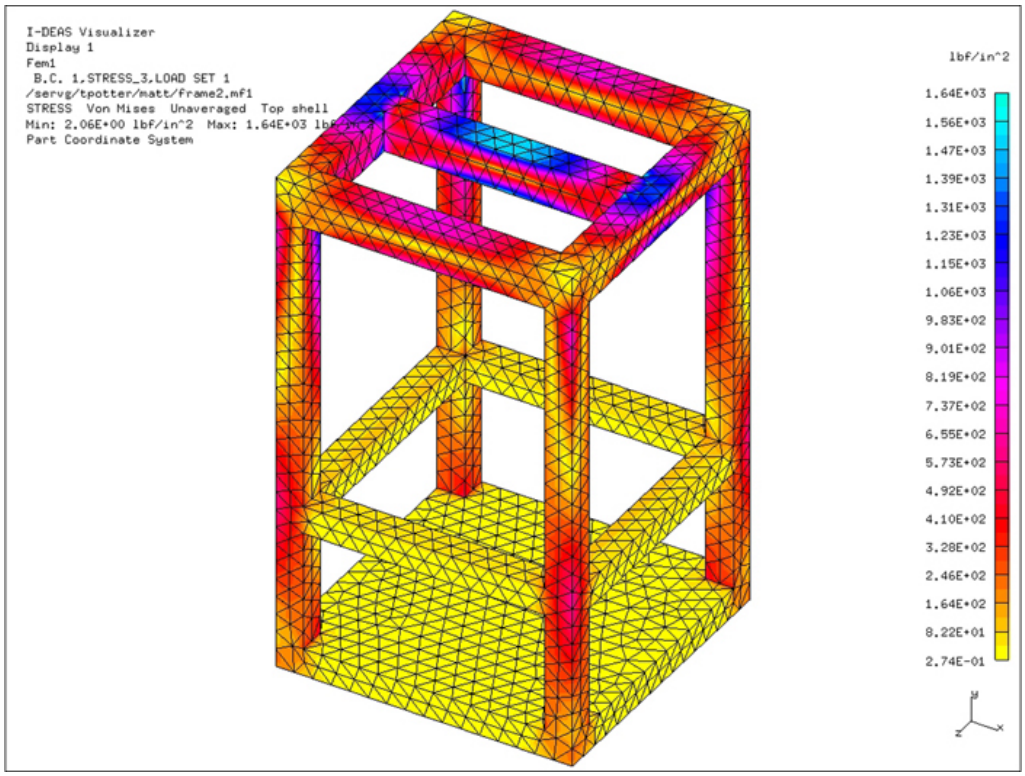

Figure 3-10. IDEAS FEA output showing areas of stress in the apparatus frame.

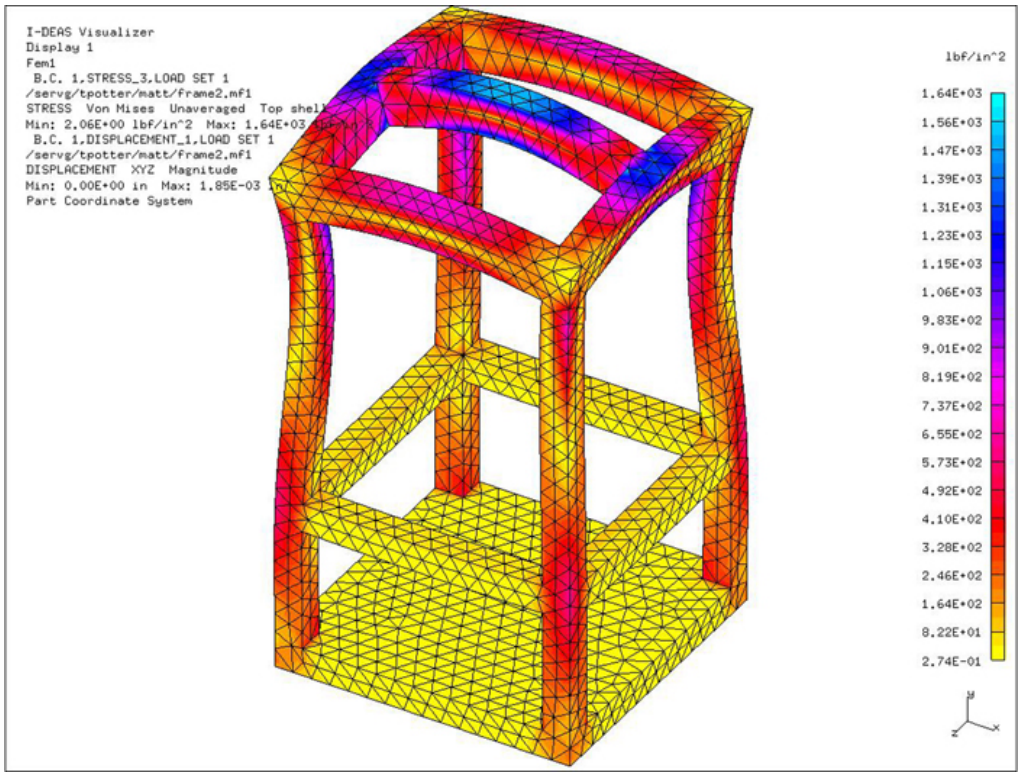

Figure 3-11. Exaggerated displacement of the frame during vertical loading of 2000 pounds.

Although the displacements of the frame may look considerable in Figure 3-11, the actual maximum displacement determined by FEA was only 0.00185 inches. In fact, the low maximum displacement and extremely low maximum stress signify that alteration of the frame will be negligible. Additionally, the minor displacement of the frame ensures that the CoCr disc will stay flush with the UHMWPE during testing to maintain equal loading across the contacting surfaces.

Simple static FEA has shown that the proposed frame should easily endure the large applied stresses, while allowing very little displacement at the material interface. Refer to Appendix H for a listing of FEA results and boundary conditions. With the frame design completed, the design and selection of the other crucial device components are subsequently discussed.

3.2.7 Apparatus Motors

Stepping motors were required for two separate operational functions of the wear testing device. Specifically, two motors were needed to simulate flexion/extension (F/E) by rotating the rods attached to the CoCr discs, and an additional two motors were necessary to control the displacements and velocities of the two linear tables responsible for AP sliding and tibial rotation. Selection of an appropriate motor depends on its capabilities and specifications, including maximum torque, required resolution, speed, source of power, and cost. Additionally, the motor requirements depend on several of the system's specifications, which are subsequently discussed.

3.2.7.1 Flexion/Extension Motors

During normal operation, each motor required for F/E must rotate two CoCr discs from 0 to 70° and back again in less than 1 second. In addition, the motors must be capable of overcoming the frictional force between the CoCr discs and the UHMWPE. Consequently, selection of the proper motor required performing several calculations, which are dependent on many properties of the system. The independent variables necessary to determine the F/E motors for the designed system are given in Table 3-6.

Table 3-6. Independent variables needed for F/E motor selection

Max loading on each F/E rod, W	1000 pounds
Coefficient of friction, μ	0.05
CoCr disc radius, R	1.25 in
Required motor resolution, θs	0.072°
CoCr density, ρ *	0.299 lb/in^3
Acceleration period, t_1	0.25 s
Positioning period, t_0	1.0 s

*Carpenter®, Reading, PA

An important step in motor selection is determining the operating pattern. As previously discussed in Section 2.1.2 and shown again in Figure 3-12, to simulate knee motion the motors are required to follow the F/E curve. Upon examination of the walking cycle for the knee, the quickest acceleration in the F/E curve is observed between toe off (T.O.) and heel strike (H.S.), when the flexion angle drops from approximately 70° to 0° in about 0.25 seconds (Lafortune *et al*., 1992). Hence, it was desired to have this acceleration capability in the F/E motors.

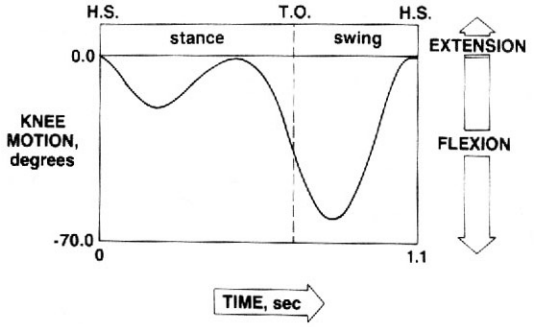

Figure 3-12. Flexion angle of the knee versus time during one walking cycle. (Lafortune *et al*., 1992)

Additionally, it was necessary to determine the torque required for the desired operation of the F/E motors prior to motor selection. Specifically, a series of calculations (Oriental Motors, Torrance, CA) were performed as outlined.

First, the number of operating pulses, A, was determined as follows:

$$A = \frac{required\ angle}{\theta s} = \frac{70°}{0.072°\ per\ pulse} = 972\ pulses \tag{3-11}$$

where A = pulses required by the motor to move 70°,
required angle = 70°, and
θs = motor resolution.

Second, the operating pulse speed, f_2, was determined as follows:

$$f_2 = \frac{A - f_1 \cdot t_1}{t_0 - t_1} = \frac{972\ pulses - 0 \cdot (0.25\,s)}{1.0\,s - 0.25\,s} = 1296\,Hz \tag{3-12}$$

where f_1 = starting pulse speed,
t_1 = acceleration period, and
t_0 = positioning period.

Calculating the required torque, T_M, involves the addition of the load torque and the acceleration torque, T_a. The load torque, T_L, is the frictional resistance produced by the contact of the CoCr and UHMWPE. The maximum load torque occurs when the joint force curve peaks (1000 pounds total for the two stations) and is determined as follows:

$$T_L = \mu \cdot W \cdot R = (0.05) \cdot (1000\,pounds) \cdot (1.25\,inches) = 62.5\,lb \cdot in \tag{3-13}$$

where μ = coefficient of friction,
W = maximum load on each rod, and
R = CoCr disc radius.

The acceleration torque, T_a is the torque required only in acceleration and deceleration operation of the motor. It is dependent on the inertia in the motor, which cannot be determined until a motor is selected.

$$T_a = \frac{J_0 + J_1}{g} \cdot \frac{\pi \cdot \theta s}{180^\circ} \cdot \frac{f_2 - f_1}{t_1} \tag{3-14}$$

where J_o = rotor inertia

J_1 = total inertia, and

g = gravitational constant (386 in/s^2).

The rotor inertia, J_0 is not yet known, however, the total system inertia, J_1, can be determined for the two CoCr discs and the F/E rod.

The inertia of a cylinder, J_x, is simply

$$J_x = \frac{\pi}{32} \cdot \rho \cdot L \cdot D^4, \tag{3-15}$$

where ρ is the material density, L is the cylinder length, and D is the cylinder diameter. The total inertia, J_1, is therefore just the summation of the inertias of the two CoCr discs and the F/E rod, which is 5/8 of an inch in diameter, 16 inches long, and made from cold-rolled steel (ρ = 0.290 lb/in^3).

$$\begin{aligned} J_1 &= 2 \cdot \left(\frac{\pi}{32} \cdot 0.299 \cdot 1.0 \cdot 2.5^4 \right) + \left(\frac{\pi}{32} \cdot 0.290 \cdot 16 \cdot \left(5\!\!\diagup\!\!8 \right)^4 \right) \\ &= 2 \cdot (1.47) + 0.0695 = 3.01 \; lb \cdot in^2 \end{aligned} \tag{3-16}$$

Solving equation 3-14 for T_a is simply,

$$\begin{aligned} T_a &= \frac{J_0 + J_1}{g} \cdot \frac{\pi \cdot \theta s}{180} \cdot \frac{f_2 - f_1}{t_1} \\ &= \frac{J_0 + 3.01}{386} \cdot \frac{\pi \cdot 0.072^\circ}{180^\circ} \cdot \frac{1296}{0.25} = 0.17 J_0 + 0.508 \, lb \cdot in \end{aligned} \tag{3-17}$$

With rotor inertias (J_0) ranging from 0.1 to 1.0 lb·in^2, it was assumed that the acceleration torque, T_a, is negligible in comparison to the load torque, T_L. Therefore, the required torque, T_M, is simply the maximum load torque of 62.5 lb·in.

To accurately select an appropriate stepping motor which fit the design specification for F/E, technical assistance from the engineers at Oriental Motors was required. Based upon their recommendation, a geared, 5-phase motor (Model #UPK596AW-T20) with a permissible torque of 104 lb·in and a 0.036° step was selected. All relevant specifications for the motor selected (UPK596AW-T20) and its speed and torque characteristics are shown in Table 3-7 and Figure 3-13, respectively.

Table 3-7. Motor specifications for the UPK596AW-T20 (Oriental Motors)

Maximum holding torque	104 lb-in
Rotor inertia	0.48 lb-in^2
Rated current	0.75 A/phase
Basic step angle	0.036°
Gear ratio	20:1
Permissible torque	104 lb-in
Power source	Single-phase 115V
Size	NEMA 43

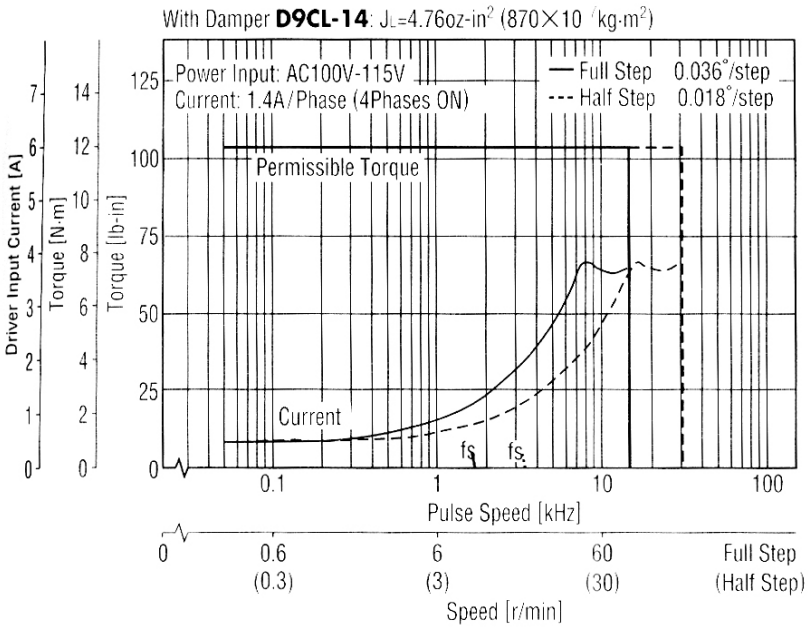

Figure 3-13. Speed vs. torque curve for the selected F/E stepper motor (UPK596AW-T20). Notice that at the maximum speed of 1296 Hz, the permissible torque is well over our maximum required torque of 62.5 lb-in (Oriental Motors catalog).

The motors selected for the F/E (UPK596AW-T20) were more than capable of supplying the maximum required torque at the maximum speed. An added benefit was the ease of accommodating the motors into the frame structure to rotate the F/E rods. The dimensions of the UPK596AW-T20 are provided in Figure 3-14. With the F/E motors decided upon, the next step was the selection of the two stepping motors responsible for moving the linear tables.

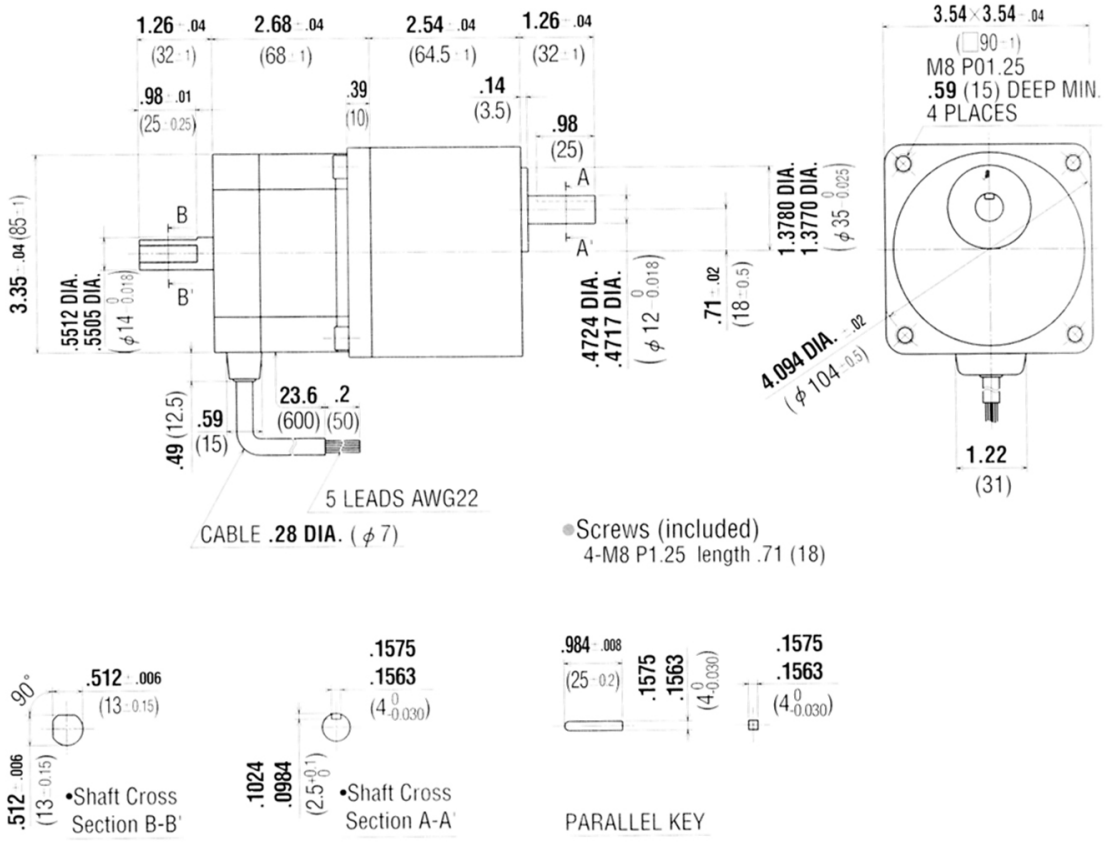

Figure 3-14. Dimensions (in inches) of the F/E motor, UPK596AW-T20. The diagram shows two shafts, although we are only concerned with the single shafted model. Values in parentheses are in millimeters. (Oriental Motors catalog)

3.2.7.2 Linear Table Motors

The two linear tables (i.e, linear guides) responsible for producing AP sliding and tibial rotation have similar travel distances and loads. Consequently, the two motors required similar torques and speeds, and therefore, identical motors were used for each table.

The steps in selecting appropriate motors for the tables are similar to the calculations used for the F/E motor. However, the linear tables add some complexity to the calculations with the conversion of the rotating motion of the motors to the linear motion of the tables by means of the ball screw assembly (Oriental Motors catalog). The ball screw added several independent variables to the motor selection process. A complete list of the variables necessary to determine the appropriate motors for the linear tables is provided in Table 3-8.

Table 3-8. Independent variables necessary for linear table motor selection.

Max loading on each table, W	1,975 pounds
Coefficient of friction of sliding surfaces, μ	0.05
Ball screw efficiency, η	0.9
Internal coefficient of friction at pilot pressure nut, μ_0	0.3
Ball screw shaft diameter, D_B	25 mm (0.98")
Total length of ball screw, L_B	325 mm (12.8")
Density of ball screw material, ρ	0.29 lb/in^3
Pitch of ball screw, P_B	5 mm (0.197")
Resolution, Δl	0.001"/step
Feed (travel distance)	25 mm (0.98")
Positioning period, t_0	1.0 s
Acceleration period, t_1	0.25 s

Since the curves for AP sliding and the simulated tibial rotation are similar to that of F/E, the acceleration period here is again 0.25 seconds. Once more, the operating pulses, A, and the maximum operating pulse speed, f_2, must be determined.

$$A = \frac{l}{P_B} \cdot \frac{360°}{\theta_s} = \frac{25\,mm}{5\,mm} \cdot \frac{360°}{0.72°} = 2500\ pulses \tag{3-18}$$

where A = pulses required by the motor to move the linear guide 25 mm,

l = feed per unit,

P_B = ball screw pitch,

θ_s = step angle.

$$f_2 = \frac{A - f_1 \cdot t_1}{t_0 - t_1} = \frac{2500\ pulses - 0 \cdot (0.25\,s)}{1.0\,s - 0.25\,s} = 3333\,Hz \tag{3-19}$$

where f_2 = maximum operating pulse speed,

f_1 = starting pulse speed,

t_1 = acceleration period, and

t_0 = positioning period.

Calculating the load torque, T_L, for the table motors was done a little differently than previously done for the F/E motors. In addition to the maximum load and sliding coefficient of friction, the load torque is dependent of several factors regarding the ball screw. The pilot pressure load, F_0, was calculated first.

$$F_0 = \frac{\mu \cdot W}{3} = \frac{0.05 \cdot 1{,}975\, pounds}{3} = 32.9\ pounds \tag{3-20}$$

where F_0 = pilot pressure load in the table,

μ = coefficient of friction on the sliding surface, and

W = maximum applied load.

$$\begin{aligned} T_L &= \frac{\mu \cdot W \cdot P_B}{2\pi \cdot \eta} + \frac{\mu_0 \cdot F_0 \cdot P_B}{2\pi} \\ &= \frac{(0.05) \cdot (1975) \cdot (0.197)}{2\pi \cdot (0.9)} + \frac{(0.3) \cdot (32.9) \cdot (0.197)}{2\pi} = 3.75\ lb \cdot in \end{aligned} \tag{3-21}$$

where μ_0 = coefficient of friction at the pilot pressure nut and

η = ball screw efficiency.

To calculate the acceleration torque, T_a, the total inertia, J_L, must be known. The total inertia is simply the summation of the ball screw inertia, J_B, and the inertia of the table and work, J_T.

$$J_B = \frac{\pi}{32} \cdot \rho \cdot L_B \cdot {D_B}^4 = \frac{\pi}{32} \cdot (0.29) \cdot (12.8) \cdot (0.98)^4 = 0.336\ lb \cdot in^2 \tag{3-22}$$

where J_B = ball screw inertia,

ρ = density of the ball screw (0.29 lb/in^3),

L_B = ball screw length, and

D_B = ball screw diameter.

$$J_T = W \cdot \left(\frac{P_B}{2\pi}\right)^2 = 1975 \cdot \left(\frac{0.197}{2\pi}\right)^2 = 1.94\ lb \cdot in^2 \tag{3-23}$$

where J_T = inertia of the table and work.

$$J_L = J_B + J_T = 0.336 + 1.94 = 2.28\ lb \cdot in^2 \tag{3-24}$$

Calculating the acceleration torque, T_a, involves the same equation (3-14) used in the F/E motor selection, with substitution of the inertias determined above. Once again, the acceleration torque is dependent on the rotor inertia, J_0, which is dependent on the type of motor selected, so that

$$\begin{aligned} T_a &= \frac{J_0 + J_L}{g} \cdot \frac{\pi \cdot \theta s}{180°} \cdot \frac{f_2 - f_1}{t_1} \\ &= \frac{J_0 + 2.28}{386} \cdot \frac{\pi \cdot 0.72°}{180°} \cdot \frac{3333}{0.25} = 0.43 J_0 + 0.99\ lb \cdot in \end{aligned} \tag{3-25}$$

Notice that unlike previously, the acceleration torque here is significant when compared to the load torque; therefore, both torques were accounted for in the determination of the total required torque, T_M.

$$T_M = T_L + T_a = 3.75 + (0.43 J_0 + 0.99) = 0.43 J_0 + 4.74\ lb \cdot in \tag{3-26}$$

Ranging from 0.1 lb-in to only 1.0 lb-in, rotor inertia did not play a part in choosing a motor capable of the required torque. Given T_M, Oriental Motors was able to help us find a motor to meet our needs. Based upon their recommendation, a 5-phase stepping motor with a maximum holding torque of 18.2 lb-in, a basic step angle of 0.72°, and a rotor inertia of 0.48 lb-in^2 (Model CSK596-NATA) was selected. Knowing J_0 , the required torque, T_M, was calculated using Equation 3-26 to be 4.95 lb-in. All relevant

specifications for the motor selected and its speed and torque characteristics are shown in Table 3-9 and Figure 3-15, respectively.

Table 3-9. Motor specifications for the CSK596-NATA. (Oriental Motors)

Maximum holding torque	18.2 lb-in
Rotor inertia	0.48 lb-in^2
Rated current	2.8 A/phase
Basic step angle	0.72°
Power source	24V DC
Size	NEMA 34

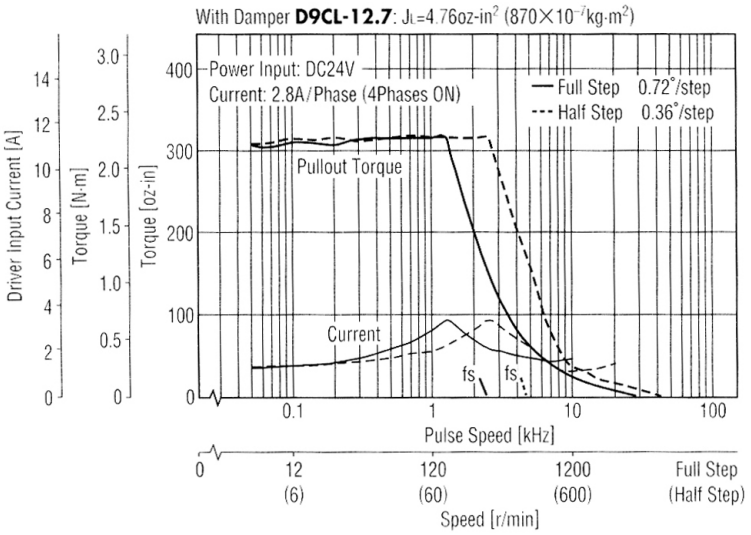

Figure 3-15. Speed vs. torque curve for the CSK596-NATA. Notice that even at our maximum required speed of 3333 Hz, our maximum required torque of 4.95 lb-in (79.2 oz-in) is within the permissible torque of the motor (Oriental Motors, Torrance, CA).

The motors selected for the linear tables (CSK596-NATA) were more than capable of supplying the maximum required torque at the maximum speed. Additionally, a major advantage of this motor was its NEMA 34 size, which fit the already selected linear tables. The dimensions of the CSK596-NATA are shown in Figure 3-16.

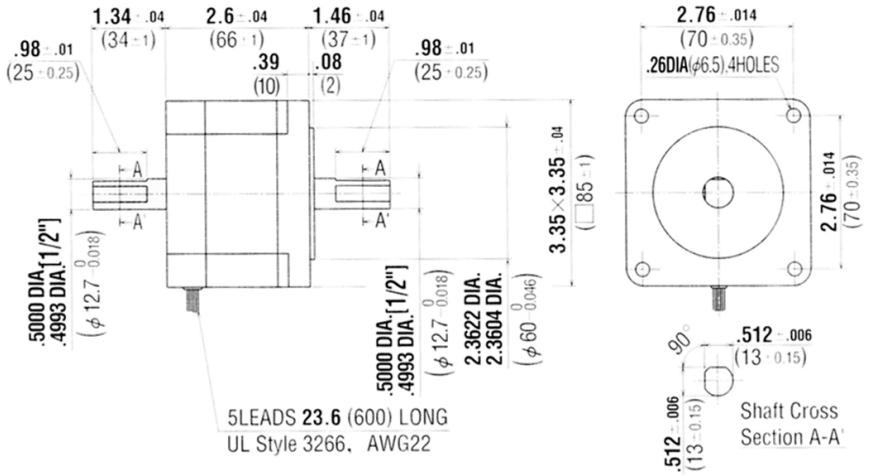

Figure 3-16. Dimensions (in inches) of the motor, CSK596-NATA, responsible for moving the two linear tables. The diagram shows two shafts, although we are only concerned with the single shafted model. Values in parentheses are in millimeters. (Oriental Motors catalog)

One additional criterion important in motor selection was the capability of all motors to be computer-controlled using Labview^{TM} (National Instruments, Austin, TX) and a motor/driver package like the one shown in Figure 3-17. Details concerning the computer set up and data acquisition are discussed in Chapter 4.

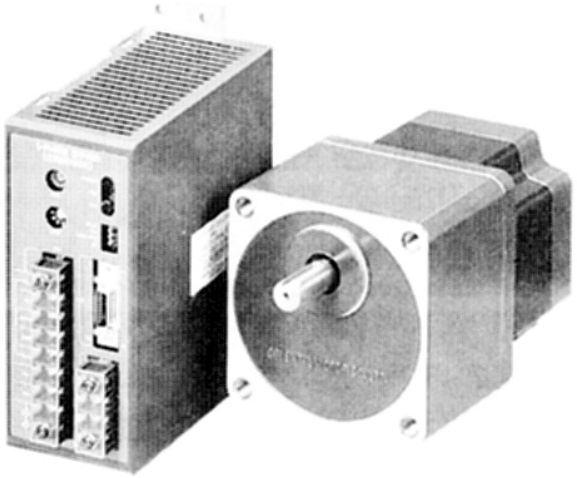

Figure 3-17. A UPK motor and driver package from Oriental Motors.

3.2.8 F/E Rod and Bearing Design

Knowing the shaft sizes for the selected F/E motors, the proper size F/E rod and bearings were determined. Due to the limited selection of motor couplings from Oriental Motors, the 12 mm (0.47") shaft size of the F/E motor (UPK596AW-T20) restricted the largest diameter of connecting equipment to 5/8 of an inch. To maintain a considerable factor of safety against yielding, an F/E rod 5/8" in diameter was chosen. Each of the two rods were 17" long and extended through two CoCr discs and three bearings, and were connected to the motors by means of flexible couplings.

As previously stated, the sleeve bearings in the initial design were replaced by pillow block bearings to allow easy insertion and adjustment of the F/E rods. Six standard pillow block bearings (VAK series) from Torrington® (Torrington, CT) with 5/8" shaft diameters and self-locking collars met the requirements, as far as load and friction were concerned. A picture of a pillow block bearing along with its dimensions is shown in Figure 3-18.

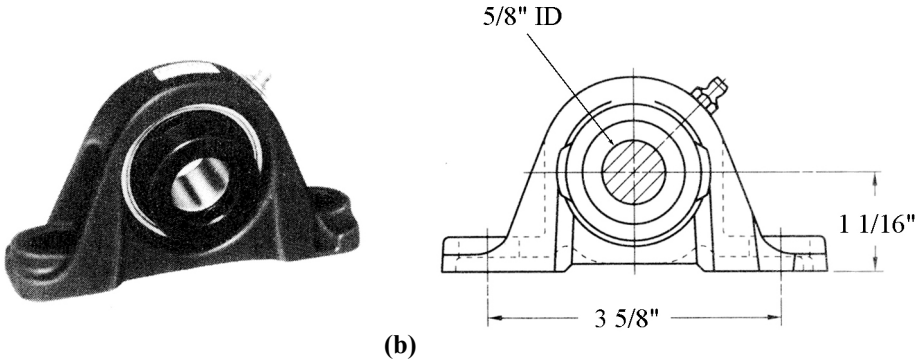

Figure 3-18. Picture (a) and relevant dimensions (b) of the VAK series pillow block bearing to be used in the wear testing device. (Torrington®, Torrington, CT)

Upon completion of the design and selection of the device's major components, the next steps included frame construction, attachment of the components via appropriate hoses and wiring, and properly interfacing the motors and valve with the computer. All of these aspects of the project are discussed in Chapter 4.